*J. Ocean Univ. China* (Oceanic and Coastal Sea Research)
DOI 10.1007/s11802-012-1910-1
ISSN 1672-5182, 2012 11 (3): 279-289
*http://www.ouc.edu.cn/xbywb/*
*E-mail:xbywb@ouc.edu.cn*

**Doctor Forum**

# Distribution of Vertical Turbulent Mixing Parameter Caused by Internal Tidal Waves and Solitary Waves in the South Yellow Sea

SI Zongshang, FAN Zhisong*, and DU Ling

*College of Physical and Environmental Oceanography*, *Ocean University of China*, *Qingdao* 266100, *P. R. China*

(Received November 12, 2011; revised February 17, 2012; accepted June 4, 2012)


**Abstract** Many observations show that in the Yellow Sea internal tidal waves (ITWs) possess the remarkable characteristics of internal Kelvin wave, and in the South Yellow Sea (SYS) the nonlinear evolution of internal tidal waves is one of the mechanisms producing internal solitary waves (ISWs), which is different from the generation mechanism in the case where the semidiurnal tidal current flows over topographic drops. In this paper, the model of internal Kelvin wave with continuous stratification is given, and an elementary numerical study of nonlinear evolution of ITWs is made for the SYS, using the generalized KdV model (GKdV model for short) for a continuous stratified ocean, in which the different effects of background barotropic ebb and flood currents are considered. Moreover, the parameterization of vertical turbulent mixing caused by ITWs and ISWs in the SYS is studied, using a parameterization scheme which was applied to numerical experiments on the breaking of ISWs by Vlasenko and Hutter in 2002. It is found that the vertical turbulent mixing caused by internal waves is very strong within the upper layer with depth less than about 30m, and the vertical turbulent mixing caused by ISWs is stronger than that by ITWs.

**Key words** internal tidal wave; internal solitary wave; vertical turbulent mixing; the South Yellow Sea

## 1 Introduction

In summer, the distribution characteristics of internal waves are quite complicated in the Yellow Sea due to the presence of the seasonal thermocline. The experiments conducted by Zhou and his group over a four-year period in the Yellow Sea showed that the frequency response of shallow water sound propagation in the summer was a strong function of time and propagation direction, and sometimes exhibited an abnormally large attenuation over some frequency range (Zhou *et al*., 1991). They investigated the possibility that the anomalous propagation results of sound were due to the presence of internal solitary waves (ISWs). Hsu *et al*. (2000) believed that the packets of ISWs in the South Yellow Sea (SYS) were generated from the islands near the southwest tip of the Korea Peninsula by the collision of the Korea coastal current and the semi-diurnal tides. Based on the SAR images and the results of the shallow water acoustics experiment in the Yellow Sea, an internal wave distribution map was given (Hsu *et al*., 2000, Fig.8), and many ISWs concentrate in the SYS. Recently, Warn-Varnas *et al*. (2005) studied the nonlinear internal waves generated by the steep topography in the southwest of the Yellow Sea (a sea area near the south of the Shandong Peninsula), using SAR technique and numerical simulation. These nonlinear internal waves propagate in the form of internal tidal waves (ITWs) in the onshore direction (westward), while in the form of ISWs in the offshore direction (eastward), which is consistent with the distribution map (Hsu *et al*., 2000, Fig.8): there were seldom eastward propagating ISWs in the southwest of the Yellow Sea. Episodes of high-frequency internal waves, which lasted approximately 3 h, were detected in the northern East China Sea during a specific phase of the barotropic tide (*i.e.*, low tide at 32˚N, 125˚E) (Lee *et al.*, 2006). The wave packets were presumably generated near the ocean shelf break approximately 200 km to the southeast of the test site, and Kelvin-Helmholtz instability may be the generation mechanism. As we all know, strong ITWs are regularly generated at the ocean shelf break in the East China Sea (Niwa and Hibiya, 2004). In addition, many observation results in the Yellow Sea (Zhao, 1992, at Station L3 (38˚32′N, 121˚07′E), Station L4 (38˚32′N, 121˚26.6′E), Station L5 (37˚49.5′N, 122˚37.4′E), Station L6 (37˚50′N, 123˚E), Station S1 (33˚17.8′N, 124˚47.5′E), Station S2 (34˚17.32′N, 122˚47.36′E), and other stations near the Laotieshan channel) showed that there were rarely ISWs at these stations except that strong nonlinear ISWs were observed at Station S1 due to the force 11 wind. Also, the dominant forms of internal waves were the linear semidiurnal and diurnal ITWs, which possess remarkable characteristics of internal Kelvin waves. The measured data was fitted by a two- or three-layer internal Kelvin wave

* Corresponding author. Tel: 0086-532-66782355
E-mail: fanzhs@ouc.edu.cn

model (Zhao, 1992).

ITWs appear to be a type of internal Kelvin wave in the Yellow Sea. The nonlinear evolution of ITWs is a generation mechanism of ISWs in the SYS, which is different from the mechanism confirmed by Warn-Varnas *et al*. (2005) that the generation and propagation of ISWs occurs when the semidiurnal tidal current flows over steep terrain. However, there are a great many of problems to be solved on the nonlinear evolution of ITWs, such as why do the ISWs concentrate in the SYS, while there are seldom ISWs in the north of the Yellow Sea? The sea area near the Laotieshan Channel is a region with many islands and large-amplitude semidiurnal and diurnal ITWs exist, but why are ISWs not generated?

In this paper, based on some observation results, a hypothetical straight wall channel is considered in the SYS, and an elementary numerical simulation of semidiurnal and diurnal ITWs along the channel is made by using the internal Kelvin wave model with continuous stratification. We obtain satisfactory results for the vertical distributions of the vertical displacement $\zeta$, the horizontal velocity $u_1$, and the vertical shear of $u_1$ for the first mode ITWs. Then, the reflection and nonlinear evolution of semidiurnal ITWs is modeled with the lateral boundary of the straight wall channel formed by the islands and coastline of the Korea Peninsula.

Furthermore, the parameterization of vertical mixing plays an important role in the Ocean Circulation Model, especially the mixing due to the ITWs and ISWs on the continental shelf. Some important results have been gained. Pacanowski and Philander (1981) used the parameterization scheme of vertical eddy mixing in the numerical model of the tropical ocean. They set the vertical eddy viscosity coefficient $A$ of momentum and the vertical eddy diffusivity coefficient $K$ of temperature in the following forms:

$$A=\frac{A_0}{(1+aRi)^n}+A_b, \tag{1}$$

$$K=\frac{A}{1+aRi}+K_b, \tag{2}$$

where $Ri$ is the Richardson number

$$Ri=\frac{BgT_z}{u_z^2+v_z^2}, \tag{3}$$

and the coefficient of thermal expansion of sea water $B$ is

$$B\sim 8.75\times10^{-6}(T+9), \tag{4}$$

where $T$ denotes the potential temperature in ℃, $T_z$ is the vertical gradient of potential temperature, $u$ and $v$ are the horizontal velocity components of equatorial ocean circulation, $u_z$ and $v_z$ are the vertical gradient of horizontal velocity components, $g$ is the gravitational acceleration, $A_b$ and $K_b$ are background dissipation parameters, and $A_0$, a and $n$ are adjustable parameters. After several numerical experiments, the optimum parameter values are set:

$A_b=1\times10^{-4}\,\mathrm{m^2s^{-1}}$, $K_b=1\times10^{-5}\,\mathrm{m^2s^{-1}}$, $n=2$, $a=5$, $A_0=\mathrm{O}(5\times10^{-3}\,\mathrm{m^2s^{-1}})$.

Compared with the interior mixing in deep ocean, the interior mixing in shallow sea area presents more remarkable regional variation and seasonal change, and the effect of ITWs and ISWs is more important. Oceanic interior mixing can be divided into two forms: vertical mixing and horizontal mixing. In many numerical models the vertical mixing process is usually parameterized in a very crude manner. Constants are often assigned to the coefficients of vertical eddy viscosity $A$ and eddy diffusivity $K$. On the broad continental shelves or marginal seas with strong stratification, the parameterization scheme of interior mixing caused by ITWs and ISWs is very important. Vlasenko and Hutter (2002) theoretically studied the breaking of ISWs using Reynolds equations. It was found that strong breaking was caused by the kinematic instability of propagating waves. At the latest stage of the evolution, the overturned hydraulic jump transformed into a horizontal density intrusion (turbulent pulsating wall jet) propagating onto the shelf. In their numerical experiments, the vertical fluid stratification and the bottom parameters were taken close to those observed in the Andaman and Sulu Seas. The breaking had been measured in the Sulu Sea (Chapman *et al.*, 1991) and the Pechora Seas (Serebryany and Shapiro, 2000). Vlasenko and Hutter (2002) modified the parameterization scheme of Pacanowski and Philander (1981), and gave a new one suitable for the propagation of ISWs. They rewrote Eq. (3) as

$$Ri=\frac{N^2}{U_z^2}, \tag{5}$$

where $U_z$ is the vertical gradient of horizontal velocity component caused by ISWs, and $N$ is the buoyancy frequency. After many numerical experiments, they found the optimum parameter values:

$A_0=10^{-3}\,\mathrm{m^2s^{-1}}$, $A_b=10^{-5}\,\mathrm{m^2s^{-1}}$, $K_b=10^{-6}\,\mathrm{m^2s^{-1}}$, $a=5$, $n=1$,

and obtained satisfactory simulation results for the breaking of ISWs. It must be emphasized that the vertical turbulent mixing caused by ISWs in the model of Vlasenko and Hutter is different from the vertical eddy mixing in the general circulation models. The former is one order of magnitude lower than the latter.

Qiao *et al*. (2004) classified the vertical dynamical mixing under four types: turbulent mixing (mixing induced by the flutter component of circulation velocity), ocean wave mixing, tidal current mixing and internal wave mixing. For the first three types, they parameterized the mixing process, and simulated the vertical temperature structure of the Yellow Sea and the East China Sea. Based on a wave-current coupled numerical model, Hu *et al*. (2004) parameterized the effect of ocean waves in the surface layer, modified the POM model, and studied the circulation and tides simultaneously in the Yellow Sea

and the East China Sea. Afterwards, an ideal numerical simulation using the POM model with an ideal topographic condition was designed by Li *et al*. (2006). They parameterized the vertical tidal mixing process and established a semiempirical formula for the vertical eddy viscosity coefficient. However, for the SYS, little attention has been paid to vertical internal wave mixing, and a proper parameterization scheme for the internal wave mixing near the thermocline has not been found as yet. In this paper, we aim at finding an appropriate parameterization scheme for the vertical turbulent mixing caused by ITWs and ISWs in the SYS without considering the breaking process of ITWs and ISWs due to kinematic instability.

The structure of the paper is as follows: The internal Kelvin Wave model is described in Section 2. In Section 3, the nonlinear evolution of ITWs is modeled using the GKdV model. Based on the previous work, the vertical turbulent mixing caused by ITWs and ISWs in the SYS is studied in Section 4 using a modified parameterization scheme of Vlasenko and Hutter (2002). The conclusions are provided in Section 5.

## 2 The Internal Kelvin Wave Model of Internal Tidal Waves

The Yellow Sea Trough is a well-known topographic feature of the Yellow Sea, which becomes shallower from south to north. The depth is 60–80 m. The topography is steep on the east side, while gentle on the west side. A hypothetical straight wall channel is considered in the SYS, as shown in Fig.1. The central axis $O-O1$ is set as the $X$-axis in the direction of 30° north by west. The $Y$-axis is perpendicular to the $X$-axis in the direction of 60° north by east. The geographic coordinates of point $O$, A and B are (34°N, 125°E), (34°4′N, 125°6′E) and (36°34′N, 123°51′E), respectively. The width of the channel is about 30km (the width between A1 and A, or B1 and B), the length is about 300 km, and the depth is 70 m. The governing equations of the internal Kelvin wave model in the Boussinesq approximation are as follows:

$$\frac{\partial u_1}{\partial t}=-\frac{1}{\rho_*}\frac{\partial p'}{\partial x}, \tag{6-1}$$

$$v=0, \tag{6-2}$$

$$fu_1=-\frac{1}{\rho_*}\frac{\partial p'}{\partial y}, \tag{6-3}$$

$$\frac{\partial w}{\partial t}=-\frac{1}{\rho_*}\frac{\partial p'}{\partial z}-\frac{\rho'}{\rho_*}g, \tag{6-4}$$

$$\frac{\partial u_1}{\partial x}+\frac{\partial w}{\partial z}=0, \tag{6-5}$$

$$\frac{\partial \rho'}{\partial t}+w\frac{\mathrm{d}\rho_0(z)}{\mathrm{d}z}=0, \tag{6-6}$$

where $oxy$ is the right hand coordinate; $z$ is a vertical coordinate and positive upward; $\rho_*$ is the reference density at the sea surface; $\rho_0(z)$ is the density distribution; $f=2\Omega\sin\varphi$ is the Coriolis parameter, where $\Omega$ is the geostrophic angular velocity and $\varphi$ is the latitude.

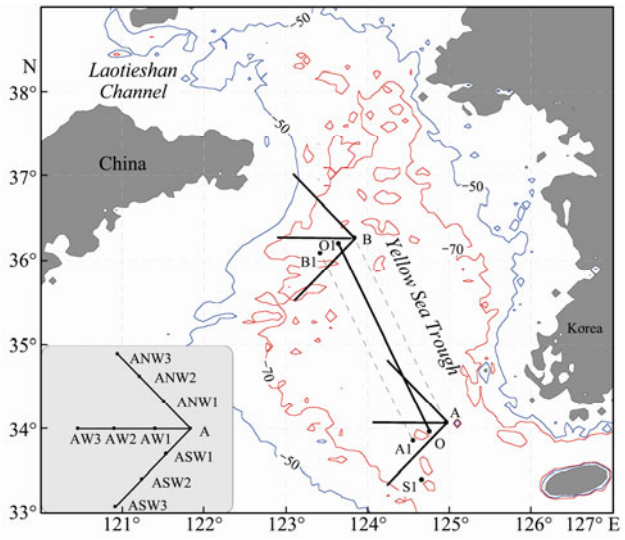


Fig.1 Map of the Yellow Sea showing bathymetries of 50 m and 70 m, and Stations A and B, as well as observation Station S1.

The solution of Eqs. (6-1)–(6-6) is in the form

$$\begin{bmatrix}u_1\\ w\\ p'\\ \rho'\end{bmatrix}=\begin{bmatrix}u_1(z)\\ w(z)\\ p'(z)\\ \rho'(z)\end{bmatrix}\cdot E\cdot\exp\left(-\frac{f}{c_1}y\right)\cdot\exp[i(kx-\omega t)], \tag{7}$$

where $E$ is the factor of amplitude, $k$ is the horizontal wave number of the internal Kelvin wave, $\omega$ is the frequency of the internal Kelvin wave, $c_1$ is the wave velocity of the internal Kelvin wave, and

$$c_1=\frac{\omega}{k}. \tag{8}$$

Thus, we can obtain

$$-i\omega u_1(z)=-\frac{ik}{\rho_*}p'(z), \tag{9-1}$$

$$fu_1(z)=\frac{f}{c_1\rho_*}p'(z), \tag{9-2}$$

$$-i\omega w(z)=-\frac{1}{\rho_*}\frac{\mathrm{d}p'(z)}{\mathrm{d}z}-\frac{g}{\rho_*}\rho'(z), \tag{9-3}$$

$$iku_1(z)+\frac{\mathrm{d}w(z)}{\mathrm{d}z}=0, \tag{9-4}$$

$$-i\omega\rho'(z)+w(z)\frac{\mathrm{d}\rho_0(z)}{\mathrm{d}z}=0. \tag{9-5}$$

After a simple algebraic deduction, the governing equation of the wave function $w(z)$ is obtained as follows:

$$\frac{\mathrm{d}^2w(z)}{\mathrm{d}z^2}+\left[\frac{N^2(z)-\omega^2}{\omega^2}\right]k^2w(z)=0, \tag{10}$$

where $N(z)$ is the Brunt-Väisälä frequency

$$N(z)=\left[-\frac{g}{\rho_*}\frac{\mathrm{d}\rho_0(z)}{\mathrm{d}z}\right]^{1/2}. \tag{11}$$

Under the rigid lid approximation, the boundary conditions of Eq. (10) are

$$w(z)=0,\ \text{at}\ \ z=0\ \ \text{and}\ \ z=-H, \tag{12}$$

$H$ being the local depth. The vertical displacement $\zeta$ of the internal Kelvin wave approximately satisfies the relation

$$w=\frac{\partial\zeta}{\partial t} \tag{13}$$

so that the wave function $\zeta(z)$ satisfies the equation in the form

$$\frac{\mathrm{d}^2\zeta(z)}{\mathrm{d}z^2}+\left[\frac{N^2(z)-\omega^2}{\omega^2}\right]k^2\zeta(z)=0, \tag{14}$$

and the boundary conditions

$$\zeta=0,\ \text{at}\ \ z=0\ \ \text{and}\ \ z=-H. \tag{15}$$

The values of $w(z)$ and $\zeta(z)$ are normalized by their maxima.

The above is the internal Kelvin wave model with continuous stratification. We notice that there is no $f$ in Eqs. (10) and (14), meaning that an internal Kelvin wave with frequencies lower than $f$ can exist.

The climatic data of temperature and salinity are downloaded from http://www.nodc.noaa.gov and used to evaluate the Brunt-Väisälä frequency $N(z)$. These data in the world ocean have a resolution of 0.25° by 0.25° grid in the horizontal and 24 layers in the vertical. The required data of 33 layers in the vertical can be obtained by interpolating from the downloaded data. The vertical profiles of temperature, salinity, density and the Brunt-Väisälä frequency $N(z)$ at Station A in August are shown in Figs.2 and 3. Whereafter, using the Thomson-Haskell calculation method (Fliegel and Hunkins, 1975), the normalized wave function $w(z)$, $\zeta(z)$ and internal Kelvin wave velocity $c_1$ can be obtained from Eqs. (10) and (14). The vertical profile of $w(z)$ (or $\zeta(z)$) for the first mode at Station A is shown in Fig.3, the corresponding $c_1$ being 0.67 m s$^{-1}$.

The largest amplitude of the ITWs at Station S1 is 5–6 m (Zhao, 1992), and the amplitude of the diurnal ITWs is larger. At Station A, the largest amplitudes of the semidiurnal and diurnal internal Kelvin waves are set equal to 5.5 m and 6 m respectively in the following modeling. Therefore, the amplitude factor $E$ in Eq. (7) is 0.89 and 0.98 respectively for the semidiurnal and diurnal internal Kelvin waves. Fig.4 shows the vertical profiles of $\zeta$ and the horizontal velocity $u_1$ on the wave hollow of the internal Kelvin wave of semidiurnal (diurnal) frequency at Station A in August. And we also obtain the vertical shear profile of the horizontal velocity $u_1$ on the wave hollow of the internal Kelvin wave of semidiurnal (diurnal) frequency (Fig.5).

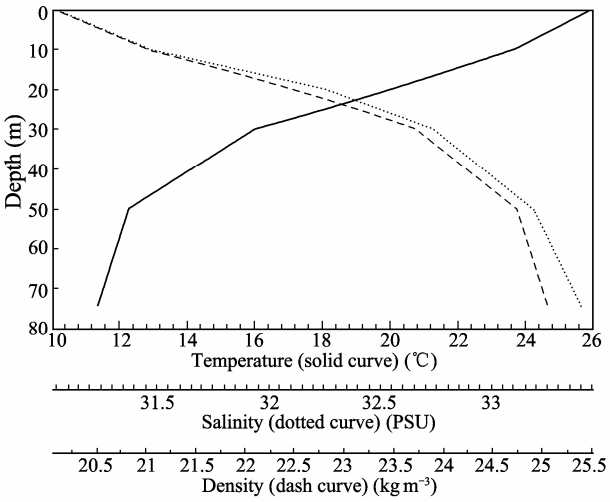


Fig.2 The vertical profiles of temperature, salinity and density at Station A in August.

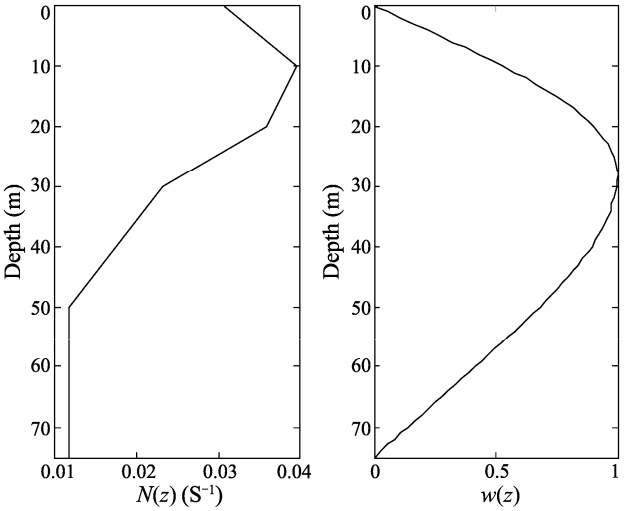


Fig.3 The vertical profile of the Brunt-Väisälä frequency $N(z)$ and the wave function $w(z)$ (or $\zeta(z)$) for the first mode at Station A in August.

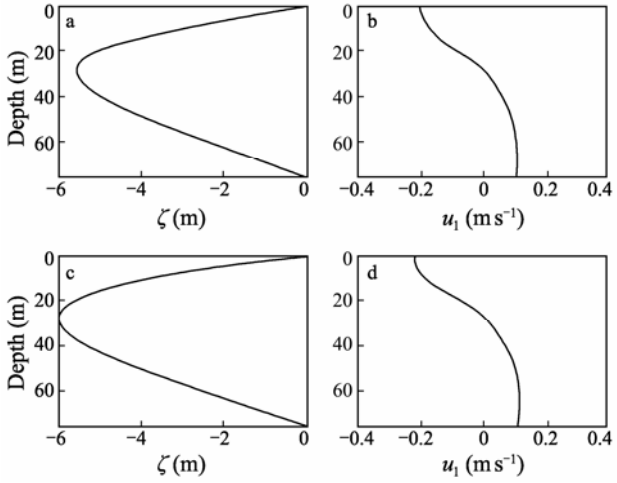


Fig.4 The vertical profiles of the displacement $\zeta$ and horizontal velocity $u_1$ on the wave hollow of internal Kelvin wave of semidiurnal or diurnal frequency at Station A in August. a, semidiurnal frequency; b, semidiurnal frequency; c, diurnal frequency; d, diurnal frequency.

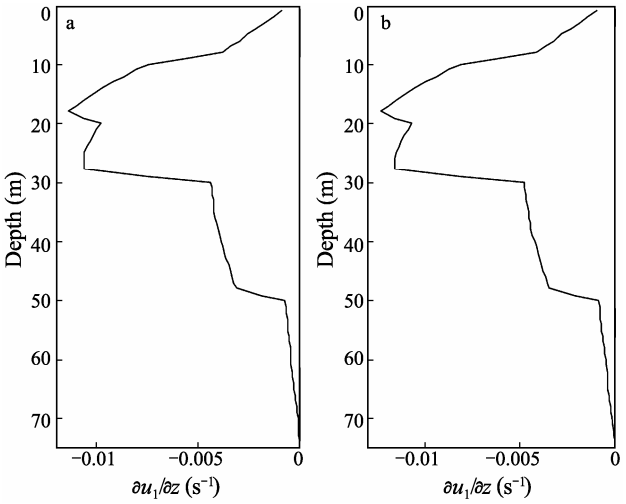


Fig.5 The vertical shear profiles of the horizontal velocity $u_1$ on the wave hollow of internal Kelvin wave of semidiurnal or diurnal frequency at Station A in August. a, semidiurnal frequency; b, diurnal frequency.

In August, strong pycnocline exists at Station A (Figs.2 and 3), and its central depth is about 15 m. Actually, in the Yellow Sea, strong pycnocline exists in the upper layer while the Yellow Sea Cold Water Mass exists at the bottom in summer. The maximum of $w(z)$ (or $\zeta(z)$) for the first mode is located at the depth 30 m approximately (Fig.3). Fig.4 shows that the positions of the maximum of the vertical displacement $\zeta$ and the turning depth of $u_1$ are all at the depth of ca 30 m. In Fig.5, the shear value (absolute value) is larger within the upper layer with depth less than about 30 m. These results are of great significance in the study of the interior mixing process and the mechanisms of the Cold Water Mass in the Yellow Sea.

## 3 GKdV Model

The reflection and nonlinear evolution of semidiurnal ITWs for the first mode at Station A and Station B in the westward, southwestward and northwestward directions are also modeled and shown in Fig.1. The physical model is the GKdV model for a continuous stratified ocean (Fan *et al.*, 2008; Fan *et al.*, 2011; Shi *et al.*, 2009a; Shi *et al.*, 2009b), in which the different effects of background ebb and flood currents are considered. This nonlinear internal wave model is a development from the work of Holloway *et al*. (1997) and Grimshaw *et al*. (2002), and is suitable for broad continental shelves or marginal seas.

### 3.1 Introduction of the GKdV Model

In fact, in the GKdV model, the vertical displacement of the isopycnal of ISWs is of the form $\eta(x, t)\Phi(z)$, where $z$ is the vertical coordinate and positive upward, $\Phi(z)$ is the vertical structure of the vertical-displacement amplitude of an internal wave mode, and $\eta(x, t)$ satisfies the GKdV equation with continuous stratification as follows (Holloway *et al*., 1997; Fan *et al*., 2008; Fan *et al*., 2011; Shi *et al*., 2009a; Shi *et al*., 2009b):

$$\frac{\partial \eta}{\partial t}+c_2\frac{\partial \eta}{\partial x}+\alpha\eta\frac{\partial \eta}{\partial x}+\beta\frac{\partial^3 \eta}{\partial x^3}+\frac{c_2}{2Q}\frac{\mathrm{d}Q}{\mathrm{d}x}\eta+\frac{\kappa c}{h^2}\eta|\eta|-\nu\frac{\partial^2 \eta}{\partial x^2}=0\,, \tag{16}$$

where $t$ is time, $x$ is the horizontal coordinate,$c_2$ is the phase speed of long internal waves, $\alpha$ is the nonlinearity coefficient, $\beta$ is the dispersion coefficient, $Q(x)$ is a result of slowly varying depth and of horizontal variability in background density and shear flow, $\kappa$ is the empirical coefficient in the quadratic bottom friction, $\nu$ is the empirical coefficient of the turbulent horizontal eddy viscosity, and $h=\sqrt{\beta/c}$ represents the vertical scale of the mode of the internal wave.

The vertical structure $\Phi(z)$ is determined by the solution of the eigenvalue problem

$$\frac{\mathrm{d}}{\mathrm{d}z}\left[(c_2-U)^2\frac{\mathrm{d}\Phi}{\mathrm{d}z}\right]+N^2(z)\Phi=0,\ \Phi(-H)=\Phi(0)=0\,, \tag{17}$$

where $N(z)$ and $U(z)$ are the Brunt-Väisälä frequency and the background current, espectively, $H$ is the local depth of seawater, and the value of $\Phi(z)$ is normalized by its maximal value. Then $\eta(x, t)$ is the isopycnal with maximal displacement.

The coefficients $\alpha$, $\beta$ and $Q$ are defined as follows:

$$\alpha=\left(\frac{3}{2}\right)\frac{\int_{-H}^{0}(c_2-U)^2(\mathrm{d}\Phi/\mathrm{d}z)^3\mathrm{d}z}{\int_{-H}^{0}(c_2-U)(\mathrm{d}\Phi/\mathrm{d}z)^2\mathrm{d}z}\,, \tag{18}$$

$$\beta=\left(\frac{1}{2}\right)\frac{\int_{-H}^{0}(c_2-U)^2\Phi^2\mathrm{d}z}{\int_{-H}^{0}(c_2-U)(\mathrm{d}\Phi/\mathrm{d}z)^2\mathrm{d}z}\,, \tag{19}$$

$$Q=\frac{c_2^2\int_{-H}^{0}(c_2-U)(\mathrm{d}\Phi/\mathrm{d}z)^2\mathrm{d}z}{c_0^2\int_{-H}^{0}(c_0-U_0)(\mathrm{d}\Phi_0/\mathrm{d}z)^2\mathrm{d}z}\,, \tag{20}$$

where the values with suffix '0' are the values at any fixed point $x_0$, and it is convenient to put $x_0$=0 at the origin (Station A or B in this work).

After taking the following substitutions

$$s=\int_0^x\frac{\mathrm{d}x}{c_2(x)}-t\,, \tag{21}$$

$$\xi=\eta\sqrt{Q(x)}\,, \tag{22}$$

Eq. (16) is reduced to

$$\frac{\partial \xi}{\partial x}+\frac{\alpha}{c_2^2\sqrt{Q}}\xi\frac{\partial \xi}{\partial s}+\frac{\beta}{c_2^4}\frac{\partial^3 \xi}{\partial s^3}+\frac{\kappa c}{\beta\sqrt{Q}}\xi|\xi|-\frac{\nu}{c_2^3}\frac{\partial^2 \xi}{\partial s^2}=0\,. \tag{23}$$

Eq. (23) is the basic equation used for the simulation of the propagation of the ISWs. After the numerical solution of Eq. (23) is obtained, the vertical displacement $\eta_1(x, s, z)$ of the isopycnal at any station ($x$) may be written in terms of Eq. (22) with the result

$$\eta_1(x,s,z)=\xi(x,s)\Phi(z)/\sqrt{Q(x)}\,. \tag{24}$$

And by using Eqs. (22) and (24) the vertical velocity $W(x, s, z)$ of the internal wave field may be approximately written as

$$W(x,s,z)=\frac{\partial\eta}{\partial t}=\frac{-\Phi(z)}{\sqrt{Q(x)}}\frac{\partial\xi(x,s)}{\partial s}\,. \tag{25}$$

According to the stream function (Holloway *et al.*, 1999)

$$\Psi(x,t,z)=c_2\eta(x,t)\Phi(z)\,, \tag{26}$$

the horizontal velocity $u_2(x, t, z)$ of the internal wave field may be approximately written as

$$u_2(x,t,z)=c_2\eta(x,t)\frac{\partial\Phi(z)}{\partial z}\,. \tag{27}$$

The propagation of an internal wave is accompanied by energy losses due to bottom friction and horizontal diffusion. The bottom turbulent boundary layer is parameterized by the empirical expression for the bottom friction stress in the Chezy form or quadratic bottom friction (Holloway *et al*., 1997):

$$\tau_b=\rho\kappa u|u|\,, \tag{28}$$

where $\rho$ is the seawater density, $u$ is the near-bottom velocity outside the boundary layer, and $\kappa$ is the empirical coefficient ($\kappa$ is about 0.001–0.0026). The empirical coefficient of the turbulent horizontal eddy viscosity $v$ has a large value in the GKdV model. Liu *et al*. (1985) used $v$=10–30 $m^2 s^{-1}$ for soliton modeling in the Sulu Sea; in a study of internal waves in the New York Bight, Liu (1988) estimated $v$ to be of the order of 1 $m^2 s^{-1}$; and Sandstrom and Oakey (1995) obtained 0.2 $m^2 s^{-1}$ as an average value of $v$ for the Scotian Shelf.

### 3.2 Model Initialization

Following the previous work, the stations in the west direction from Station A are designated as AW, AW1, AW2, and AW3, respectively. Correspondingly, the stations are ASW, ASW1, ASW2, and ASW3 in the southwest direction and ANW, ANW1, ANW2, and ANW3 in the northwest direction. The distance is about 27.5 km between two westward stations and about 38.9 km between two southwestward (or northwestward) stations. Actually, the geographic coordinates of Stations AW, ASW and ANW are the same as those of Station A, that is, (34˚4′N, 125˚6′E). The purpose is just to distinguish the different propagating directions of internal waves and the different background currents. For Station B, the definition of each station and the distance between two stations are similar to the above. In the GKdV model, the origin of coordinates is set at Station A (or Station B), and the positive direction of the $x$-axis is westward (or southwestward, northwestward).

The background current is composed of the monthly mean baroclinic circulation and the barotropic tidal current. The monthly mean baroclinic circulation is the modeling results of the LICOM1.0 (Liu *et al.*, 2004; Liu *et al.*, 2005), which is a quasi-global (75˚S–65˚N) model with a uniform horizontal resolution of 0.5˚ by 0.5˚ grid. Then the modeled results are interpolated onto 0.25˚ by 0.25˚ grid. Fig.6 shows the distribution of surface current of baroclinic circulation in August in the Yellow Sea. The vertical profiles of the $U$ component of baroclinic circulation at Stations A and B are shown in Fig.7. From Figs.6 and 7 we can see that the baroclinic circulation intensity is significantly different between Stations A and B. At Station A it is about one order of magnitude larger than that at Station B. The barotropic tidal current is the modeled results of the barotropic POM model in the China Sea (24˚–41˚N, 117˚–131˚E) (Du, 2005), and only $M_2$, $S_2$, $K_1$ and $O_1$ constituents are taken into account. The modeling results have a uniform resolution of 1/6˚ by 1/6˚ grid in the horizontal and are calculated for surface, middle and bottom layers in the vertical according to $\sigma$ coordinate (the value of $\sigma$ is 0.0, −0.3, and −1.0 respectively). The $U$ ($V$) components of tidal current in the surface layer in August are shown in Figs.8 and 9. It is found that semidiurnal tidal current is dominant in the SYS, and the tidal current intensity at Station A is 2 times larger than that at Station B. Because the difference among the three layers is very small, we will adopt the surface layer result as a characteristic value of barotropic tidal current in the following numerical simulation.

In fact, the climatic data of temperature and salinity as well as the distribution of the monthly mean baroclinic circulation all present similar characteristics from June to September in the Yellow Sea. Therefore, in this paper, we take the climatic data and modeling results in August as representative in summer in the SYS.

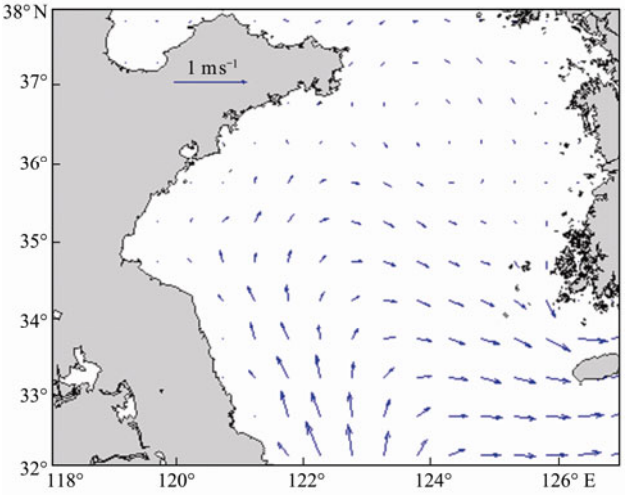


Fig.6 The distribution of surface current of baroclinic circulation in August in the Yellow Sea.

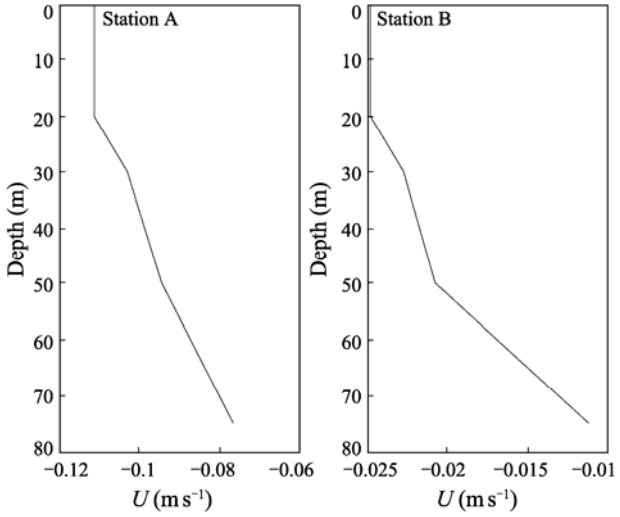


Fig.7 The vertical profiles of the U component of baroclinic circulation at Stations A and B in August.

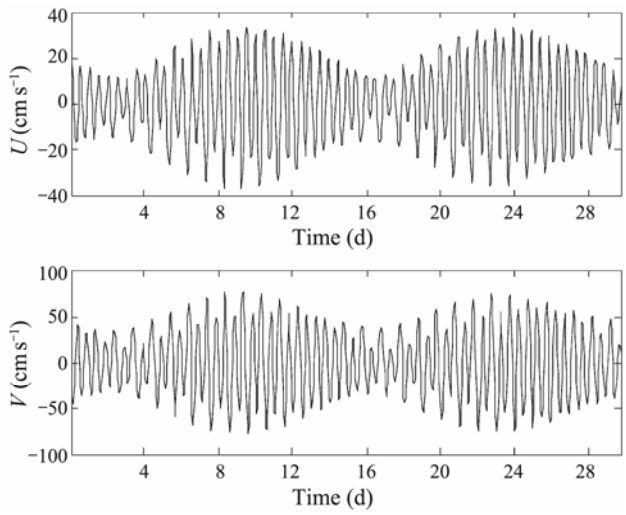


Fig.8 The modeling results of the $U$ and $V$ components of tidal current in the surface layer in August at Station A.

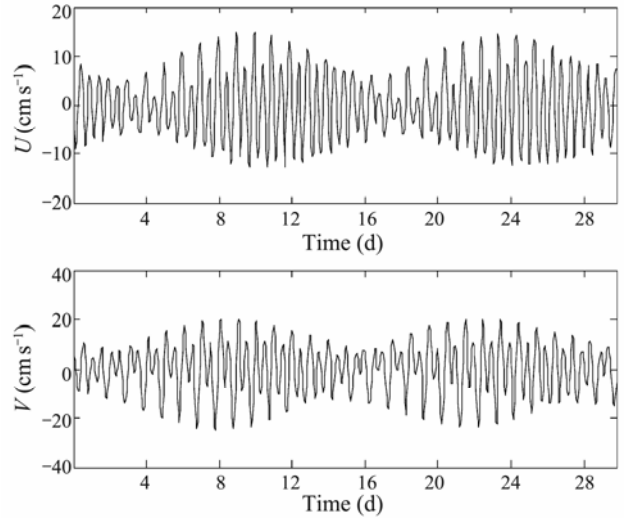


Fig.9 The modeling results of the $U$ and $V$ components of tidal current in the surface layer in August at Station B.

We choose the maximum value (the absolute value) of barotropic flood (ebb) tidal current (relative to the west coast of the Korea Peninsula) as the characteristic tidal current at each station (Table 1, barotropic tidal current). Then, the composed result of the characteristic tidal current and the monthly mean baroclinic circulation is taken as the background current at each station to calculate $\alpha$, $\beta$ and $Q$. However, a special case happens at Stations ANW, ANW1, ANW2, and ANW3 (Table 1). That is, the absolute value of barotropic tidal current is larger than the phase speed $c_2$ of long internal waves. For example, at Station ANW, the maximal value of barotropic flood current is $-0.75\,\mathrm{m\,s^{-1}}$ (listed in parentheses in Table 1), while $c_2$ is $0.469\,\mathrm{m\,s^{-1}}$. So the background current (not listed in Table 1) is $-0.88\,\mathrm{m\,s^{-1}}$, and its absolute value is larger than $c_2$, hence the ITWs are unstable (Grimshaw *et al.*, 2002; Fan *et al.*, 2011). We do not consider this unstable state in this paper. Therefore, the background currents at

Table 1 The stations and the parameters used in the modeling of nonlinear evolution of the internal tidal wave from Station A in the west, southwest and northwest directions respectively

| Station | Barotropic tidal current (m s$^{-1}$) | | Background current (m s$^{-1}$) | | $\alpha$ (s$^{-1}$) | | $\beta$ (m$^3$ s$^{-1}$) | | $c_2$ (m s$^{-1}$) |
|---|---|---|---|---|---|---|---|---|---|
| | Flood | Ebb | Flood | Ebb | Flood | Ebb | Flood | Ebb | |
| AW | −0.37 | 0.33 | −0.48 | 0.23 | −0.034 | −0.010 | 253.397 | 66.692 | 0.482 |
| AW1 | −0.24 | 0.33 | −0.35 | 0.22 | −0.030 | −0.010 | 216.438 | 67.429 | 0.486 |
| AW2 | −0.24 | 0.29 | −0.35 | 0.18 | −0.031 | −0.012 | 215.352 | 77.811 | 0.490 |
| AW3 | −0.35 | 0.29 | −0.46 | 0.18 | −0.036 | −0.013 | 242.996 | 78.030 | 0.496 |
| ANW | (−0.75)<br>−0.33 | (0.70)<br>0.29 | −0.46 | 0.16 | −0.031 | −0.011 | 242.087 | 78.388 | 0.469 |
| ANW1 | (−0.49)<br>−0.19 | (0.70)<br>0.29 | −0.32 | 0.16 | −0.027 | −0.011 | 204.017 | 78.021 | 0.464 |
| ANW2 | (−0.49)<br>−0.19 | (0.50)<br>0.25 | −0.31 | 0.13 | −0.028 | −0.013 | 203.376 | 88.735 | 0.483 |
| ANW3 | (−0.70)<br>−0.32 | (0.50)<br>0.25 | −0.41 | 0.14 | −0.035 | −0.014 | 235.924 | 89.280 | 0.511 |
| ASW | −0.46 | 0.35 | −0.49 | 0.32 | −0.041 | −0.009 | 264.981 | 58.043 | 0.552 |
| ASW1 | −0.35 | 0.35 | −0.39 | 0.31 | −0.037 | −0.010 | 238.318 | 59.843 | 0.546 |
| ASW2 | −0.35 | 0.42 | −0.40 | 0.37 | −0.037 | −0.007 | 239.834 | 43.175 | 0.545 |
| ASW3 | −0.43 | 0.42 | −0.49 | 0.36 | −0.012 | −0.002 | 120.387 | 13.095 | 0.466 |

Table 2 The stations and the parameters used in the modeling of nonlinear evolution of the internal tidal wave from Station B in the west, southwest and northwest directions respectively

| Station | Barotropic tidal current ($m\,s^{-1}$) | | Background current ($m\,s^{-1}$) | | $\alpha$ ($s^{-1}$) | | $\beta$ ($m^3\,s^{-1}$) | | $c_2$ ($m\,s^{-1}$) |
|---|---|---|---|---|---|---|---|---|---|
| | Flood | Ebb | Flood | Ebb | Flood | Ebb | Flood | Ebb | |
| BW | −0.13 | 0.14 | −0.15 | 0.12 | −0.031 | −0.019 | 167.096 | 101.880 | 0.539 |
| BW1 | −0.12 | 0.14 | −0.15 | 0.11 | −0.013 | −0.008 | 78.261 | 45.750 | 0.478 |
| BW2 | −0.12 | 0.08 | −0.15 | 0.05 | −0.013 | −0.009 | 78.261 | 53.280 | 0.474 |
| BW3 | −0.13 | 0.08 | −0.17 | 0.04 | −0.013 | −0.009 | 80.077 | 53.820 | 0.475 |
| BNW | −0.17 | 0.05 | −0.20 | 0.02 | −0.033 | −0.023 | 177.218 | 123.936 | 0.534 |
| BNW1 | −0.10 | 0.05 | −0.12 | 0.03 | −0.014 | −0.010 | 74.448 | 55.769 | 0.476 |
| BNW2 | −0.10 | 0.19 | −0.12 | 0.17 | −0.016 | −0.008 | 72.930 | 37.043 | 0.470 |
| BNW3 | −0.17 | 0.19 | −0.18 | 0.18 | 0.010 | 0.003 | 23.719 | 7.412 | 0.340 |
| BSW | −0.19 | 0.18 | −0.19 | 0.18 | −0.034 | −0.017 | 179.731 | 91.219 | 0.557 |
| BSW1 | −0.08 | 0.18 | −0.09 | 0.17 | −0.030 | −0.018 | 153.083 | 91.187 | 0.554 |
| BSW2 | −0.08 | 0.11 | −0.09 | 0.10 | −0.014 | −0.009 | 73.614 | 49.958 | 0.498 |
| BSW3 | −0.19 | 0.11 | −0.21 | 0.09 | −0.016 | −0.009 | 87.726 | 50.387 | 0.493 |

these four stations are made up of a small characteristic value of barotropic tidal current and the monthly mean baroclinic circulation. The values of background currents in the sea surface layer, the nonlinear coefficient $\alpha$, the dispersion coefficient $\beta$, and the phase speed $c_2$ of long internal waves are listed in Tables 1 and 2. In Table 1, the value (absolute value) of $\alpha$ on the flood is about 3 times larger than that on the ebb at each station. In addition, by comparing the results in Tables 1 and 2, the absolute value of $\alpha$ in Table 1 (the south of the SYS) is about 2–3 times larger than that at the corresponding station in Table 2 (the north of the SYS).

## 4 Modeling Results of the GKdV Model

According to the observation results (Zhao, 1992), in terms of Eqs. (7) and (8) in the paper of Holloway *et al*. (1997) and the modeling results in Section 2, we assume $\eta(x, t)$ to be of a sinusoidal waveform with 5.5 m initial amplitude at each initial station (Stations AW, ASW, ANW, BW, BSW and BNW).

A diagnostic modeling is performed in this paper. We assume there are four conditions of background currents in the nonlinear evolution of ITWs in every direction: (1) every station is on the flood (relative to the west coast of the Korea Peninsula); (2) every station is on the ebb; (3) the first and the third stations are on the ebb, while the second and the fourth stations are on the flood; (4) the first and the third stations are on the flood, while the second and the fourth stations are on the ebb. To be brief, only the nonlinear evolution processes of ITWs for the first mode from Station A in the west direction are given as shown in Figs.10–13. And the results in the northwest (southwest) direction are similar. In addition, the results corresponding to conditions (1) and (2) of background currents from Station B in the west direction are given in Figs.14 and 15. All the other results at Station B are similar. The waveform of the internal waves shown in these figures is represented with the displacement $\eta(x, t)$ of isopycnal at the depth of the maximum $\Phi(z)$ ($\Phi(z)$=1) for the first mode.

The modeling results with the GKdV model are con-

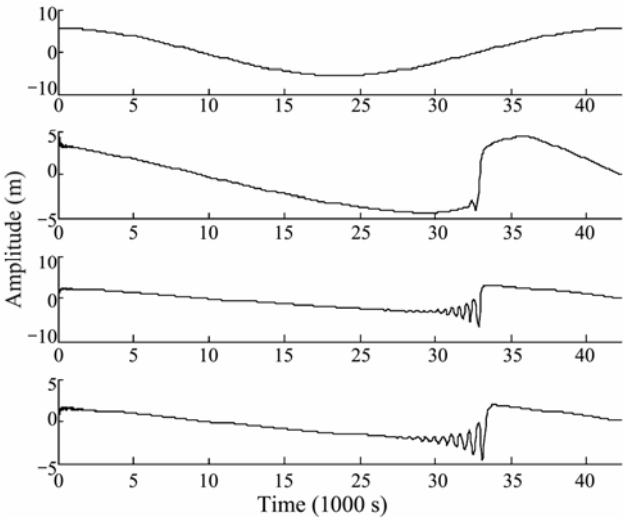


Fig.10 The displacement $\eta(x, t)$ of isopycnal of semidiurnal internal tidal wave at the depth of the maximum of $\Phi(z)$ ($\Phi(z)$=1) for the first mode. From top to bottom panels in the figure, four combinations of station and background current state are given: AW (on the flood), AW1 (on the flood), AW2 (on the flood) and AW3 (on the flood).

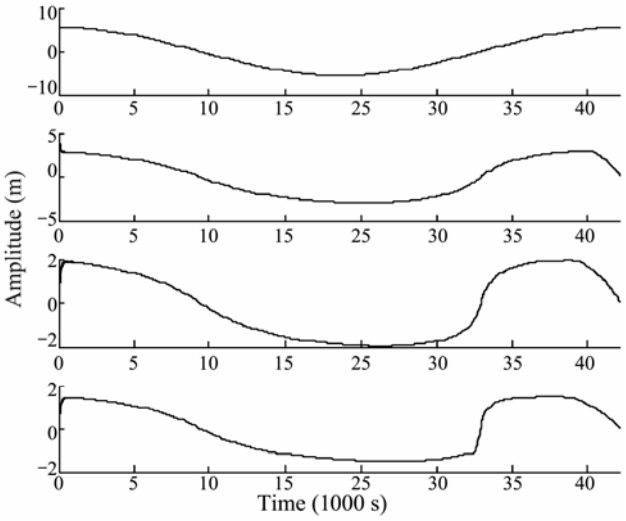


Fig.11 As in Fig.10, the four combinations of station and background current state are given: AW (on the ebb), AW1 (on the ebb), AW2 (on the ebb) and AW3 (on the ebb).

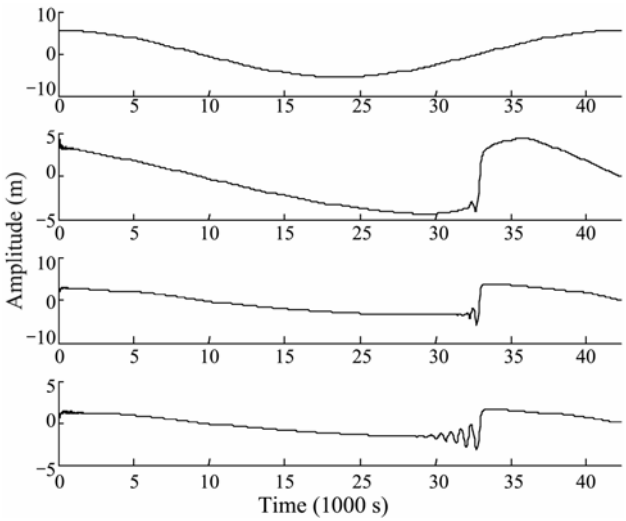


Fig.12 As in Fig.10, the four combinations of station and background current state are given: AW (on the ebb), AW1 (on the flood), AW2 (on the ebb) and AW3 (on the flood).

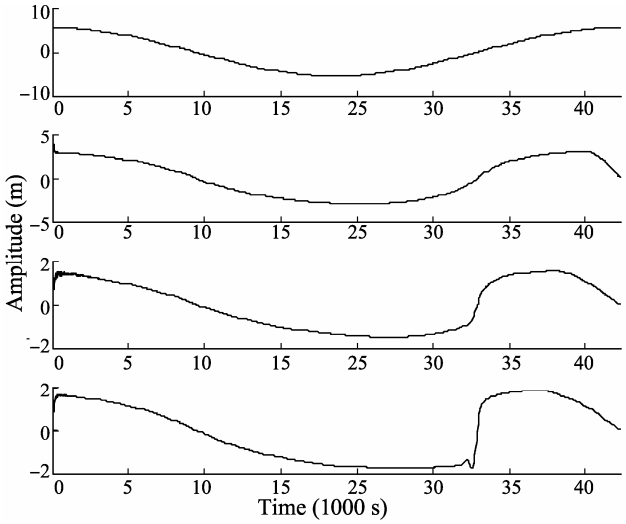


Fig.13 As in Fig.10, the four combinations of station and background current state are given: AW (on the flood), AW1 (on the ebb), AW2 (on the flood) and AW3 (on the ebb).

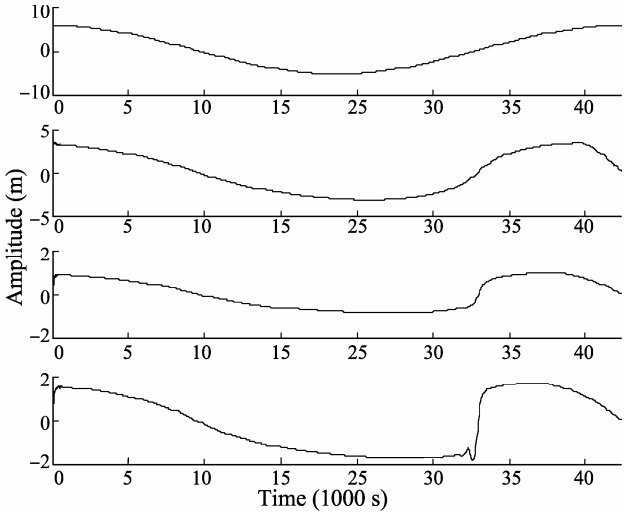


Fig.14 As in Fig.10, the four combinations of station and background current state are given: BW (on the flood), BW1 (on the flood), BW2 (on the flood) and BW3 (on the flood).

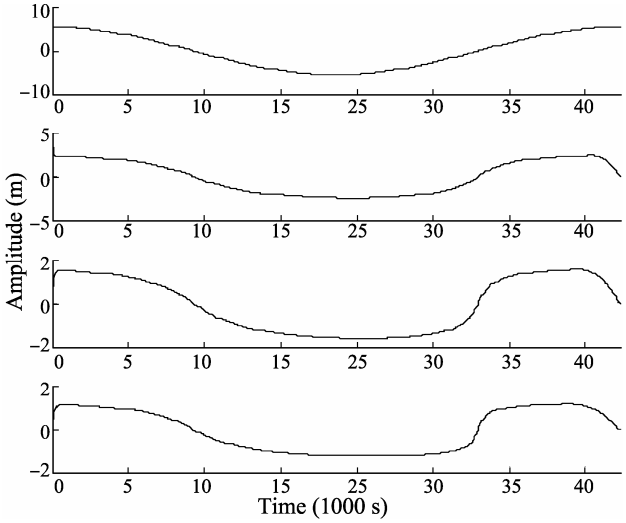


Fig.15 As in Fig.10, the four combinations of station and background current state are given: BW (on the ebb), BW1 (on the ebb), BW2 (on the ebb) and BW3 (on the ebb).

sistent with the properties of the nonlinear coefficient $\alpha$ in Tables 1 and 2. In the south of the SYS, when every station is on the flood or Station AW3 is on the flood, the westward propagating ITWs from Station A experience obvious nonlinear fission, and ISWs are generated (Figs.10 and 12). Otherwise, the ITWs are linear essentially, and only slight nonlinear changes occur (Figs.11 and 13). In the north of the SYS, the westward propagating ITWs from Station B do not show obvious nonlinear fission, even if every station is on the flood (Figs.14 and 15).

## 5 A Parameterization Scheme of Vertical Turbulent Mixing

In Sections 2 and 3, the internal Kelvin wave model for continuous stratification is given, and an elementary numerical study of nonlinear evolution of ITWs is made in the SYS. On this basis, the parameterization of vertical turbulent mixing caused by ITWs and ISWs is studied.

Based on the satisfactory modeling results of the vertical gradient of the horizontal velocity component of ITWs and ISWs, we utilize the vertical turbulent mixing scheme of Vlasenko and Hutter to study the parameterization of vertical turbulent mixing caused by ITWs and ISWs in the SYS. Following Eqs.(1), (2) and (5) and using the results of the GKdV model shown in Figs.10 and 15, we parameterize the vertical turbulent mixing of ITWs and ISWs in a semidiurnal tide cycle at Stations AW3 and BW3 respectively. In Fig.10, the initial ITWs transform into ISWs, and the parameterization results are shown in Figs.16 and 17. In Fig.15, the initial ITWs do not produce fission process, and the waveform is still that of ITWs with the parameterization results shown in Figs.18 and 19.

From Figs.16–19 it can be seen that the coefficients of vertical turbulent mixing caused by ITWs and ISWs have lager values within the upper layer with depth less than 30 m in the SYS. This result indicates that the vertical

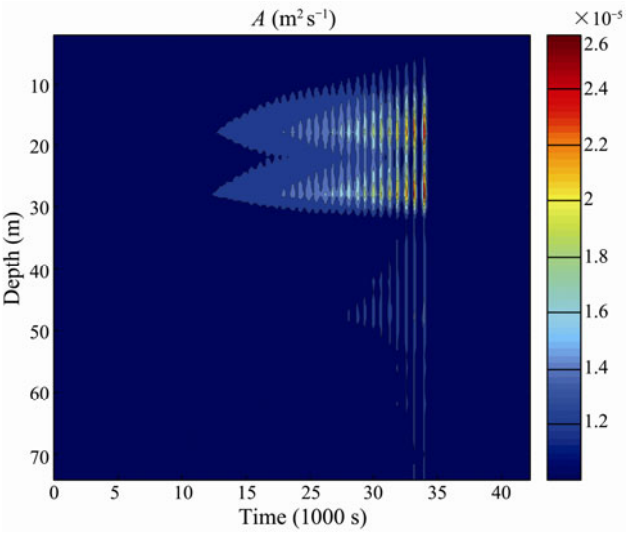


Fig.16 The distribution of vertical turbulent viscosity coefficient $A$ induced by internal solitary waves in a semi-diurnal tide cycle at Station AW3.

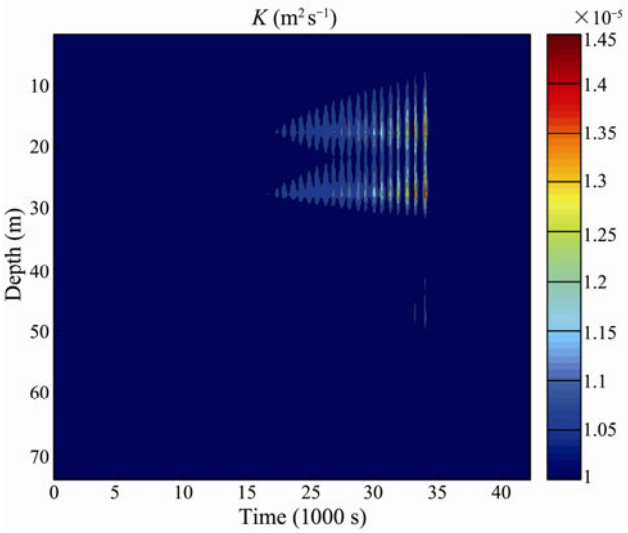


Fig.17 The same as in Fig.16, but for the distribution of vertical turbulent diffusivity coefficient $K$.

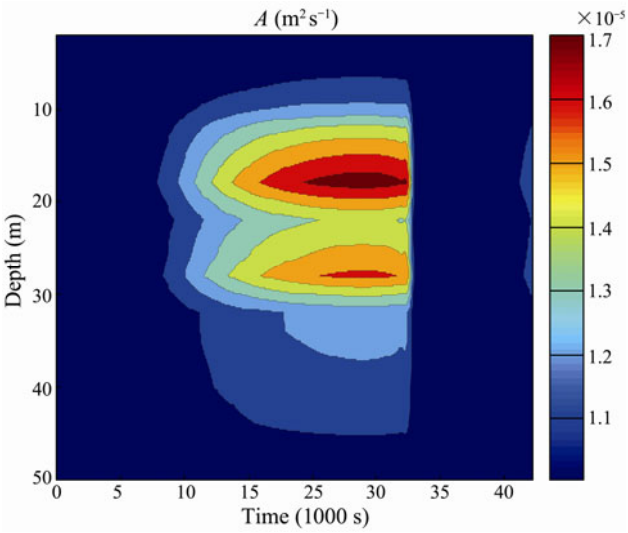


Fig.18 The distribution of vertical turbulent viscosity coefficient $A$ induced by internal tidal waves in a semi-diurnal tide cycle at Station BW3.

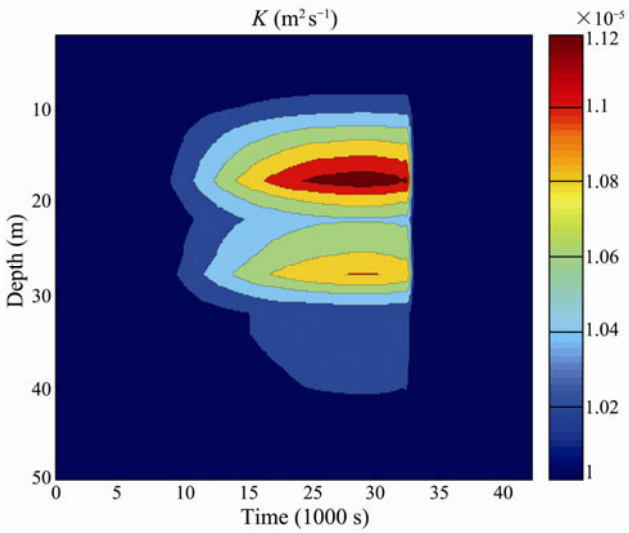


Fig.19 The same as in Fig.18, but for the distribution of vertical turbulent diffusivity coefficient $K$.

turbulent mixing in the SYS mainly concentrates in the upper water column (above depth about 30 m), which is significant for the study of the stability of the Yellow Sea Cold Water Mass and the interior mixing process caused by ITWs and ISWs. In addition, $A$ and $K$ obviously depend on the vertical gradient of the horizontal velocity component $u$ induced by ITWs and ISWs. In Figs.16 and 17, the extreme values of the coefficients $A$ and $K$ for ISWs appear alternatively, which are mutually corresponding to the peak values of ISWs. The maximum values of $A$ and $K$ are $0.274\times10^{-4}$ m$^2$ s$^{-1}$ and $0.148\times10^{-5}$ m$^2$ s$^{-1}$ respectively for ISWs, and $0.175\times10^{-4}$ m$^2$ s$^{-1}$ and $0.113\times10^{-5}$ m$^2$ s$^{-1}$ respectively for ITWs. The vertical turbulent mixing of ISWs is stronger than that of ITWs.

## 6 Conclusions

ITWs appear to be a type of the internal Kelvin wave in the Yellow Sea. The nonlinear evolution of ITWs is a generation mechanism of ISWs in the SYS. An elementary numerical simulation of the semidiurnal and diurnal ITWs along a hypothetical straight wall channel is made, using the internal Kelvin wave model with continuous stratification. By using the GKdV model, the reflection and nonlinear evolution of semidiurnal ITWs for the first mode from Station A (34˚4′N, 125˚6′E) and Station B (36˚34′N, 123˚51′E) is modeled in the west, southwest and northwest directions respectively. Moreover, the vertical turbulent mixing caused by ITWs and ISWs in the SYS is studied with a modified parameterization scheme on the basis of the work by Vlasenko and Hutter (2002). The conclusions are

a) The background currents play a very important role in the propagation processes of ITWs and ISWs. Distinguishing the different effects of the background ebb and flood currents is necessary, which is the advantage of the GKdV model.

b) The main reason that ISWs concentrate in the south of the SYS and seldom exist in the north of the SYS is the

impact of strong background baroclinic circulation and barotropic tidal current, as well as the directions of the two currents are the same on the flood (relative to the west coast of the Korea Peninsula). As a result, the nonlinear coefficient $\alpha$ of the GKdV model has a large value in this circumstance. However, these two currents are weak in the north of the SYS.

c) The vertical turbulent mixing caused by ITWs and ISWs in the SYS mainly concentrates in the upper water column (above depth about 30 m), and the vertical turbulent mixing caused by ISWs is stronger than that by ITWs.

## Acknowledgements

This work is supported by the Key Program of the National Natural Science Foundation of China under contract No. 41030855.

## References

Chapman, D. C., Giese, G. S., Collins, M. G., Encarnacion, R., and Jacinto, G., 1991. Evidence of internal swash associated with Sulu Sea solitary waves? *Continental Shelf Research*, **11**: 591-599.

Du, L., 2005. Global sea level variation and tidal waves in special regions of the China Sea. Doctor thesis. Ocean University of China, Qingdao, 158pp

Fan, Z. S., Shi, X. G., Liu, A. K., Liu, H. L., and Li, P. L., 2013. Effects of tidal currents on nonlinear internal solitary waves in the South China Sea. *Journal of Ocean University of China*, in press.

Fan, Z. S., Zhang, Y. L., and Song, M., 2008. A study of SAR remote sensing of internal solitary waves in the north of the South China Sea: I. Simulation of internal tide transformation. *Acta Oceanologica Sinica*, **27** (4): 39-56.

Fliegel, M., and Hunkins, K., 1975. Internal wave dispersion calculated using the Thomson-Haskell method. *Journal of Physical Oceanography*, **5**: 541-548.

Grimshaw, R., Pelinovsky, E., and Poloukhina, O., 2002. Higher-order Korteweg-de Vries models for internal solitary waves in a stratified shear flow with a free surface. *Nonlinear Processes in Geophysics*, **9**: 221-235.

Holloway, P. E., Pelinovsky, E., and Talipova, T., 1999. A generalized Korteweg-de Vries model of internal tide transformation in the coastal zone. *Journal of Geophysical Research*, **104**: 18333-18350.

Holloway, P. E., Pelinovsky, E., Talipova, T., and Barnes, B., 1997. A nonlinear model of internal tide transformation on the Australian North West Shelf. *Journal of Physical Oceanography*, **27**: 871-896.

Hsu, M. K., Liu, A. K., and Liu, C., 2000. A study of internal waves in the China Seas and Yellow Sea using SAR. *Continental Shelf Research*, **20**: 389-410.

Hu, H. G., Yuan, Y. L., and Wan, Z. W., 2004. Study on hydrodynamic environment of the Bohai Sea, the Huanghai Sea and the East China Sea with wave-current coupled numerical mode. *Acta Oceanologica Sinica*, **26** (4): 19-32 (in Chinese).

Lee, J. H., Lozvatsky, I., Tang, S.-T., Jang, C. J., Hong, C. S., and Fernando, H. J. S., 2006. Episodes of nonlinear internal waves in the northern East China Sea. *Geophysical Research Letters*, **33**, L18601, DOI: 10.1029/2006GL027136.

Li, M. L., Hou, Y. J., and Qiao, F. L., 2006. Parameterization of tide induced vertical eddy viscosity. *Progress in Natural Science*, **16** (1): 55-60 (in Chinese).

Liu, A. K., 1988. Analysis of nonlinear internal waves in the New York Bight. *Journal of Geophysical Research*, **93** (C10): 12317-12329.

Liu, A. K., Holbrook, J. R., and Apel, J. R., 1985. Nonlinear internal wave evolution in the Sulu Sea. *Journal of Physical Oceanography*, **15**: 1613-1624.

Liu, H. L., Li, W., and Zhang, X. H., 2005. Climatology and variability of the Indonesian Throughflow in the eddy-permitting oceanic GCM. *Advances in Atmospheric Sciences*, **22** (4): 496-508.

Liu, H. L., Yu, Y. Q., Li, W., and Zhang, X. H., 2004. *Reference Manual for LASG/IAP Climate System Ocean Model* (*LICOM 1.0*). Science Press, Beijing, 107pp (in Chinese).

Niwa, Y., and Hibiya, T., 2004. Three-dimensional numerical simulation of M2 internal tides in the East China Sea. *Journal of Geophysical Research*, **109**, C04027, DOI: 10.1029/2003 JC001923.

Pacanowski, R. C., and Philander, S. G. H., 1981. Parameterization of vertical mixing in numerical models of tropical oceans. *Journal of Physical Oceanography*, **11**: 1443-1451.

Qiao, F. L., Ma, J., Xia, C. S., Yang, Y. Z., and Yuan, Y. L., 2004. Influence of the wave induced mixing and tidal mixing on the vertical temperature structure in the Yellow Sea and the East China Sea in summer. *Progress in Natural Science*, **14** (12): 1434-1441 (in Chinese with English abstract).

Sandstrom, H., and Oakey, N. S., 1995. Dissipation in internal tides and solitary waves. *Journal of Physical Oceanography*, **25**: 604-614.

Serebryany, A. N., and Shapiro, G. I., 2000. Overturning of soliton-like internal waves: Observations on the Pechora Sea Shelf. *Fifth International Symposium on Stratified Flows*. University of British Columbia, Vancouver, BC, Canada, 1029-1034.

Shi, X. G., Fan, Z. S., and Li, P. L., 2009b. The Impact of barotropic tidal current on the simulation of large-amplitude internal solitary waves in the deep sea in the Northeast South China Sea. *Periodical of Ocean University of China*, **39** (supll. II): 297-302 (in Chinese with English abstract).

Shi, X. G., Fan, Z. S., and Liu, H. L., 2009a. A numerical calculation method of eigenvalue problem of nonlinear internal waves. *Journal of Hydrodynamics*(*Serial B*), **21** (3): 373-378.

Vlasenko, V., and Hutter, K., 2002. Numerical experiments on the breaking of solitary internal waves over a slope-shelf topography. *Journal of Physical Oceanography*, **32**: 1779-1793.

Warn-Varnas, A. C., Chin-Bing, S. A., King, D. B., Hawkins, J. A., Lamb, K. G., and Teixeira, M., 2005. Yellow Sea oceanic-acoustic solitary wave modeling studies. *Journal of Geophysical Research*, **110**, C08001, DOI: 10.1029/2004JC 002801.

Zhao, J. S., 1992. A study of internal waves in the shallow sea. In: *Oceanography in China (3)*. China Ocean Press, Beijing, 102pp (in Chinese).

Zhou, J. X., Zhang, X. Z., and Rogers, P. H., 1991. Resonant interaction of sound wave with internal solitons in the coastal zone. *Journal of the Acoustical Society of America*, **90** (4): 2042-2054.

**(Edited by Xie Jun)**